applied optics

Simple parametric model for intensity calibration of Cassini composite infrared spectrometer data

J. Brasunas,[1,*] A. Mamoutkine,[2] and N. Gorius[3]

[1]NASA Goddard Space Flight Center, Code 693, Greenbelt, Maryland 20771, USA
[2]Adnet Systems, 8800 Greenbelt Road, Code 693, Greenbelt, Maryland 20771, USA
[3]Catholic University, 8800 Greenbelt Road, Code 693, Greenbelt, Maryland 20771, USA
*Corresponding author: john.c.brasunas@nasa.gov

Received 29 February 2016; revised 18 April 2016; accepted 10 May 2016; posted 11 May 2016 (Doc. ID 260157); published 7 June 2016

Accurate intensity calibration of a linear Fourier-transform spectrometer typically requires the unknown science target and the two calibration targets to be acquired under identical conditions. We present a simple model suitable for vector calibration that enables accurate calibration via adjustments of measured spectral amplitudes and phases when these three targets are recorded at different detector or optics temperatures. Our model makes calibration more accurate both by minimizing biases due to changing instrument temperatures that are always present at some level and by decreasing estimate variance through incorporating larger averages of science and calibration interferogram scans.

OCIS codes: (140.3490) Lasers, distributed-feedback; (120.6085) Space instrumentation; (120.6200) Spectrometers and spectroscopic instrumentation; (300.6300) Spectroscopy, Fourier transforms.

http://dx.doi.org/10.1364/AO.55.004699

1. INTRODUCTION

A linear Fourier-transform spectrometer (FTS) such as Cassini composite infrared spectrometer (CIRS) [1–3] is calibrated via two calibration targets [typically deep space (cold, 3 K) and an optics-temperature shutter (warm, 170 K)] to infer response and self-emission terms. Each spectral-resolution element is statistically independent and can be calibrated separately. The fundamental requirement for accurate calibration of CIRS data is thermal stability since self-emission usually dominates external emission from Saturn, Titan, etc. Calibration is straightforward if conditions (response, self-emission, sampling comb) are stationary during the acquisition of shutter, deep-space, and science interferogram scans. Calibration can then be performed by acquiring science and calibration scans over a short time period with near-stationary conditions (the so-called local calibration). If we wish to incorporate science and calibration scans over a longer time period (a so-called global calibration), we must model changes in response, self-emission, and the sampling comb. Even for the local calibration there is likely some temperature change. Therefore our model has the promise of making both local and global calibration more accurate by minimizing biases due to changing instrument temperatures and by decreasing estimate variance by incorporating larger averages of science and calibration scans.

Since the CIRS beam splitter has absorption there is not a one-to-one correspondence between a change in the location of the interferogram center burst, which denotes the zero path difference (ZPD) point and a change in the sampling comb. Emissions from the two FTS input ports have distinct ZPD locations, and a so-called vector calibration is required [4,5]. A previous paper (hereafter referred to as the ZPD paper) described the behavior over time of the CIRS sampling comb [6]. This paper will present a model of the self-emission and response terms parametrized in terms of the dependence of raw calibration-target spectra on CIRS housekeeping data. The process of intensity calibration also brings to bear an additional mathematical constraint that enables improved estimation of sampling comb changes.

2. CIRS INSTRUMENT

The CIRS (Fig. 1) records interferometric data in one direction of travel of its moving mirror at nearly constant speed. CIRS has two distinct FTS's sharing a common moving mirror mechanism with separate moving mirrors on either end of this mechanism. Figure 1 is a simplified drawing. The mid-infrared (MIR) return mirrors are cube corners and the far-infrared (FIR) return mirrors are dihedrals. The FIR FTS includes FP1 (focal plane 1, 10 to 700 cm^{-1}) and is a polarizing design. The MIR FTS includes FP3 (566–1132 cm^{-1}) and FP4 (1019–1529 cm^{-1}) with distinctly lower temperature detectors and a conventional amplitude-division beam splitter (KBr). CIRS is temperature-controlled with internal heaters for quasi-stationary operating conditions. The noise is mostly detector Johnson (resistance) noise and there are also narrow-band interferences due to

1559-128X/16/174699-07 Journal © 2016 Optical Society of America

Corrected 6 July 2016

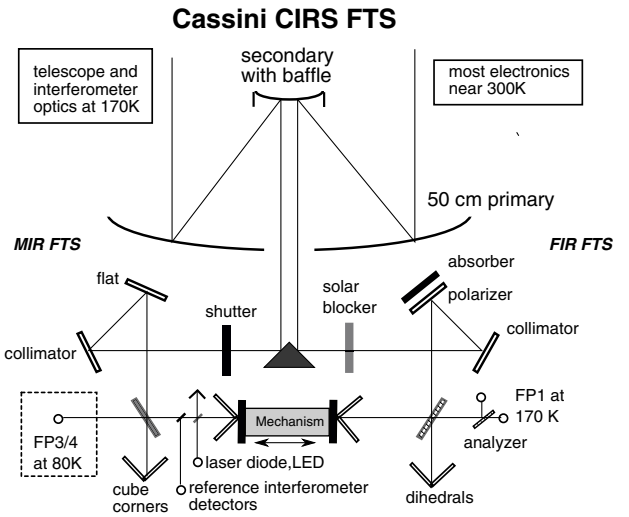

Fig. 1. Layout of CIRS telescope primary and secondary, calibration shutter, MIR FTS, FIR FTS, and detector focal planes.

spacecraft or instrument currents seen via shared grounding circuits. The mostly one-sided scan length can be changed, and the corresponding range of spectral resolution is around 15 to 0.5 cm^{-1} (apodized, Rayleigh resolution criterion), taking about 2 to 50 seconds per scan. The two-sided part of the interferogram corresponds to the lower resolution.

The ZPD paper describes the various contributors to changes in the FP4 MIR ZPD location. These are summarized below in Table 1 and listed from largest to smallest effect (random variations). The random variations are uncorrelated among the simultaneously sampled detectors unlike the true sampling comb changes. The random variations are especially high for certain values of the spacecraft reaction-wheel rates [6], therefore these data are not included in the present analyses.

Both the optics temperature, T_{OPT}, and the focal plane (FP) ¾ temperature, T_{FP}, are controlled within a narrow temperature range most of the time with occasional excursions on an approximate hourly to daily time scale in addition to a long-term drift. Table 2 summarizes the temperature behavior for the Saturn phase of the Cassini mission.

Table 1. Drivers for Changes in ZPD Location

Phenomenon	Sampling Comb Change?	Time Scale
Target effect via anomalous phase	No	Minutes to hours
Isolated changes	Yes, shift	Isolated scan or two
Laser mode change	Yes, stretch	~ yearly step change
Long term drift	Yes, shift	Multi-year to decade
Optics temperature gradient change	Yes, shift	Minutes to hours
Random variations	No	Scan to scan changes

Table 2. Time Behaviour of CIRS Thermal Zones

Temperature Zone	T_{OPT}	T_{FP}
Nominal temperature	169.79 K	76.3 K
Central spread of data	0.01 K	0.01 K
Larger daily variations	0.15 K	~3 K
10-year drift	−0.02 K	+0.025 K

3. INTENSITY CALIBRATION AT FIXED CIRS TEMPERATURES

In addition to daily and long-term drifts in T_{OPT} and T_{FP} there are long-term drifts in ZPD position and occasional changes in laser mode. If we restrict our initial attention to year 2011 data we may ignore the long-term drifts and initially work within a single laser mode. There are also the abrupt, single-scan shift anomalies, which we identify in an early processing stage and either correct or reject. If we further restrict our attention to the core, ~0.01 K spreads in T_{OPT} and T_{FP} then we may assume the chirping, emissivities, detector responsivity, FTS fringe efficiency, and beam splitter (B/S) properties including anomalous phase are essentially constant.

To perform the intensity calibration we calculate the following averages of unapodized raw spectra:

– S1, the complex Fourier transform of a large number of deep-space calibration scans at low resolution (the two-sided part);

– S2, the complex Fourier transform of a large number of shutter-closed calibration scans at low resolution;

– S3, sample-shifted complex Fourier transform of the available number of target scans at the desired resolution, apodizing if necessary to avoid double-counting of the two-sided part of the interferogram versus the single-sided part (note that the S3 scans can be anything, either calibration or science target).

An FTS such as CIRS typically has two entrance ports (one outward looking) and two output ports (Fig. 2) and not all are necessarily distinct. Without beam B/S absorption, emission from the two input ports is 180 deg out of phase. This is the scalar case. The measured interferogram may not be symmetric but this is due to chirping and sampling, which give the same phase to both entrance ports but not changing the 180-deg phase difference. It is legitimate to symmetrize the

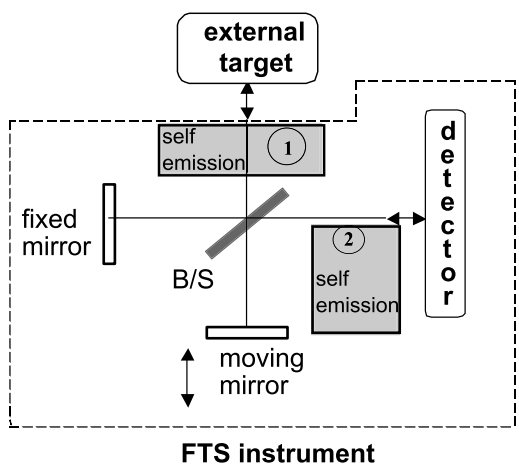

Fig. 2. Model for FTS internal emission from entrance port (1) and detector port (2).

interferogram completely removing the phase. When B/S absorption is present, emission terms from the two input ports and from the B/S no longer satisfy the scalar criterion. This is the vector case. It is as though the different emission terms contribute interferograms with different ZPD locations, in which case the interferogram is no longer inherently symmetric. It is no longer legitimate to completely phase correct the data.

However, under our restricted condition of constant instrument conditions, we can covert calibration to scalar calibration by computing the differences (S3–S1) and (S2–S1). The differencing eliminates the self-emission terms leaving only a contribution from port 1 beyond the shutter. We have thus eliminated the multiple ZPD's making CIRS amenable to scalar calibration. We may eliminate phase due to chirping and to missing the central maximum by computing the normalized ratio,

$$\mathrm{calspec}_{\mathrm{norm}}(\sigma) = \frac{S3 - S1}{S2 - S1}. \tag{1}$$

Note that $\mathrm{calspec}_{\mathrm{norm}}$ equals unity for $S3 = S2$, which is a blackbody at temperature T_{opt}. As a linear system, we may produce a calibration estimate calspec (with dimensions watts per unit area per steradian per wavenumber) as follows:

$$\mathrm{calspec}(\sigma) = \mathrm{calspec}_{\mathrm{norm}}(\sigma) B(\sigma, T_{\mathrm{opt}}), \tag{2}$$

or

$$\mathrm{calspec}(\sigma) = \frac{S3 - S1}{S2 - S1} B(\sigma, T_{\mathrm{opt}}), \tag{3}$$

where $B(\sigma, T_{\mathrm{opt}})$ is the Planck function at wavenumber σ and temperature T_{opt}. calspec is our estimate for spectral radiance from a beam-filling target; $\mathrm{calspec}_{\mathrm{norm}}$ represents the spectral radiance estimate divided by the Planck spectral radiance at the CIRS optics temperature. It is dimensionless but its units are not arbitrary.

Equations (1)–(3) become real quantities, apart from noise effects, when the instrument parameters are fixed, and the S1, S2, and S3 interferograms are restricted to their two-sided parts. The division completes the phase correction and symmetrizes calspec. Only the difference terms can be fully phase corrected. Individual S1, S2, S3 terms are governed by vector calibration and may only be partially phase corrected (phase proportional to σ). The parameter most likely to be different is the sampling shift for S3, since S1 and S2 are computed from large averages over equivalent conditions. During the calibration process S3 is partially phase-corrected to null out the imaginary part while restricted to the two-sided part of S3 scans. Then Eqs. (1)–(3) are recomputed with partially phase-corrected S3 at high resolution (mostly one-sided scan) followed by taking the real part as the calibrated spectrum. When performing the second calibration step at high spectral resolution the interferograms for S1 and S2 are zero-filled to the same length. This matches both the spectral resolution of S1, S2, S3 and length-dependent normalization factors in the discrete Fourier transform.

To assess the accuracy of our calibration we will consider the normalized calibration $\mathrm{calspec}_{\mathrm{norm}}$ for CIRS FP4 detector 25 (ZPD paper). Unless stated otherwise we will also use only the two-sided part of S3 interferograms. If the S3 scan is shutter closed, the expected answer is unity plus a random noise term. The expected answer for deep-space S3 scan is zero plus the random noise. Figure 3 shows the raw spectral amplitudes S1 (gray) and S2 (black) from early 2011. Normalized calibration of deep-space S3 from late 2011 is shown in Fig. 4. Normalized calibration of shutter-closed S3 from late 2011 is shown in Fig. 5. The real parts are, as expected, with a very small shift adjustment required to minimize the imaginary parts (Table 3).

We next calibrate shutter-closed scans from 2008 (same laser mode as 2011), 2009 (one laser-mode hop from 2011), and 2006 (two laser-mode hops from 2011). The fractional change in laser wavelength is small compared with the fractional spectral resolution of the two-sided part of the interferograms so it is reasonable to approximate the resultant sampling-comb stretch as a shift. Table 3 shows the shift parameters needed to minimize the imaginary part of the calibrated spectra. The resulting normalized calibration spectra for 2008, 2009, and 2006 are shown in Fig. 6.

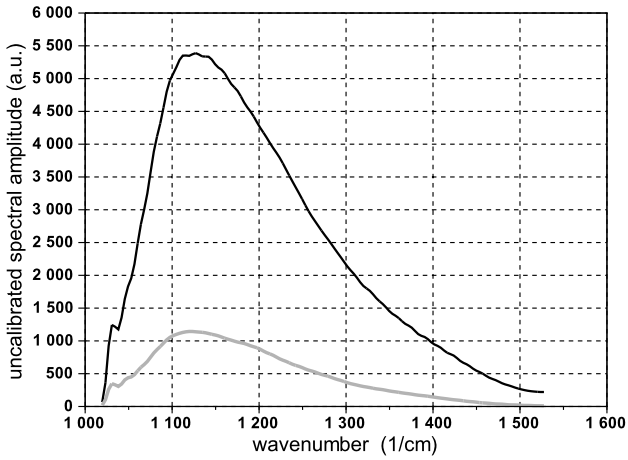

Fig. 3. CIRS FP4 early 2011 spectra: deep space S1 (gray) and shutter-closed S2 (black).

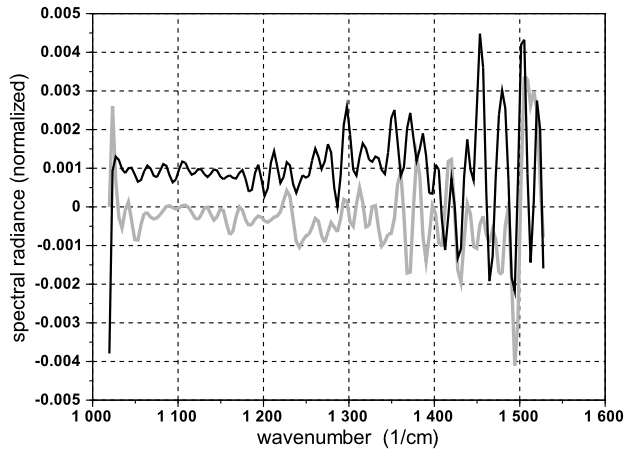

Fig. 4. Normalized spectral radiance for late 2011 deep-space scans, real (black), and imaginary (gray).

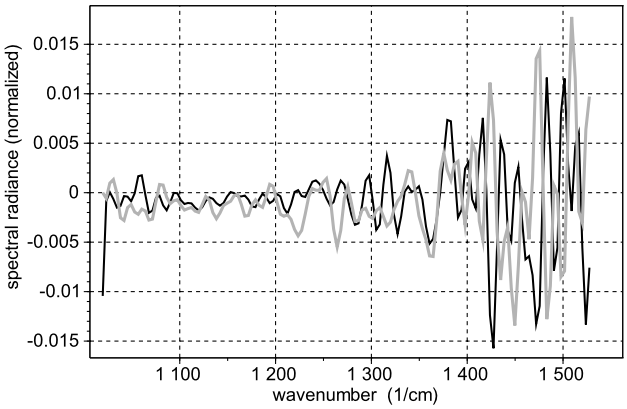

Fig. 5. Normalized spectral radiance for late 2011 shutter-closed scans: real-1 (black) and imaginary (gray).

Table 3. Shifts Needed to Calibrate Different Years (S1 and S2 from 2011)

S3 Year	α_{sh}	Δ (Laser Mode)
2011	−0.000004	0
2008	−0.00004	0
2009	−0.00011	1
2006	−0.00022	2

The time evolution of the shift parameter shown in Table 3 is as expected. A relatively small shift is needed within 2011, and a larger shift is needed to calibrate 2008 data with 2011 calibration scans due to long-term drift. 2009 and 2006 require yet larger shifts because the effective shift due to a laser mode change is large compared with the year-to-year drift. Table 3 does not show a time trend because the dominant effect is due to laser-mode hops, which do not change linearly with time but instead do a sort of random walk. Figure 6 shows that the majority of FP4 can be calibrated with calibration scans from a single year, which means separate calibration sets are not

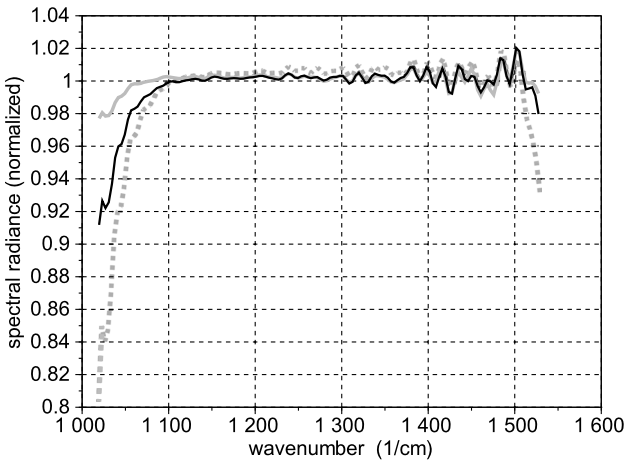

Fig. 6. Normalized spectral radiance for shutter-closed S3 scans (real part) from 2008 (solid gray–same mode), 2009 (black–one laser mode hop), and 2006 (dotted gray–two laser mode hop); S1 and S2 calibration scans are from 2011.

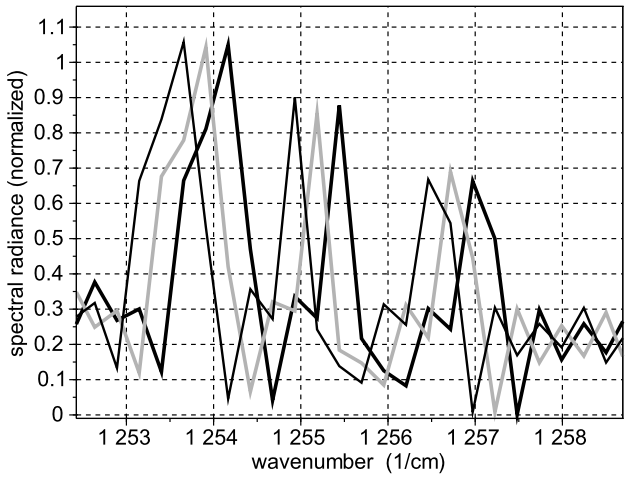

Fig. 7. Normalized spectral radiance (real part) with external targets (shutter open) in 2008 (black), 2009 (gray) and 2006 (dotted black); apodized only against double-counting.

needed for each laser mode. Using a single calibration set does introduce additional errors below 1100 cm^{-1} but this is also an area that suffers from aliasing and the Gibbs' phenomenon. The error seems to scale with how different the laser mode is for the target (S3) scans versus the calibration scans (S1 and S2) rather than aging.

Figure 7 demonstrates normalized calibration of CIRS highest spectral-resolution data, again using 2011 calibration scans to calibrate data from various years. S1 and S2 are low-resolution and S3 is high resolution with an external target in the field-of-view. First, S3 is calibrated using only the two-sided scan to enable calculation of the shift needed to zero out the imaginary part. Then the full-resolution normalized calibration is calculated with the shift just derived, and the calibrated spectrum is the real part. The apparent wavenumber change in the methane lines shows that the fractional change in wavelength between adjacent laser longitudinal modes is ∼1/5000. Also note that the final tweaking of sampling shift for the S3 target scans serves to mitigate the sometimes-seen baseline error (target radiance going negative beyond noise fluctuations).

4. DEPENDENCE OF RAW INTERFEROGRAMS AND SPECTRA ON CIRS TEMPERATURES

We have an abundance of S1 and S2 calibration scans, the majority of which are in a ∼0.01 K core region (our standard temperatures). We can afford to reject calibration scans outside the core region. We do not have this freedom with science target scans (S3). Therefore our goal is to counteract temperature effects in either S3 or S1 scans in the numerator of Eqs. (1)–(3) so that self-emission nulls out. Temperature dependence can come in through many factors. As shown in Fig. 1 CIRS has three temperature zones: the MIR detectors near 80 K (T_{FP}); most optics near 170 K (T_{OPT}); and most electronics near 300 K. To determine which housekeeping temperatures we must include in our model we examined the dependence of interferogram center-burst amplitude on housekeeping temperatures. The CIRS raw data have been interpolated to

produce the following estimates (Figs. 8 and 9) of center-burst amplitude (see ZPD paper), one dot per scan. The one recorded focal-plane temperature has been used to produce Fig. 8. For the optics temperature there are multiple sensors. The sensor in the MIR FTS near the 80 K stage (Fig. 1) has been used to produce Fig. 9.

A linear correction accounts for the observed trend of center-burst amplitude on both focal-plane temperature and optics temperature as shown in Figs. 8 and 9. Once the linear correction has been made for the optics temperature there does not appear to be any remaining dependence on the 300 K electronics temperature nor on any of the other 170 K–stage sensors. However there is a small subset of the data with elevated telescope temperatures where deep-space and shutter-closed amplitudes no longer track due to excess emission from the telescope assembly from either planetary or solar heating. These data are excluded by rejecting the data with elevated secondary-mirror baffle temperature (Fig. 1).

To gain further insight into the mechanism of center-burst temperature dependence we plot the ratio of averages of large numbers of raw spectral amplitudes of shutter-closed calibration scans at nominal focal-plane temperature (76.324 K) and elevated temperature (77.7 K), which are all from 2011 for CIRS detector 25 (Fig. 10). Since the radiance near 77 K in the FP 4 bandpass is negligible compared with emission from 170 K surfaces, we conclude any temperature dependence is due to a change in response and not in self-emission. The form of the ratio in Fig. 10 is suggestive of a dependence on the infrared detector through a temperature dependence of the low-wavenumber cutoff, plus a slight temperature dependence at higher wave numbers. We express this temperature dependence through a multiplicative term det25(σ, T) where

$$\det 25(\sigma, T) = \{C1 + \tanh[(\sigma - \sigma_c)/\mathrm{BW}]\} \times [1 + 0.003(T - 76.324)]. \quad (4)$$

We model the higher wavenumber temperature dependence (possibly due to a change in quantum efficiency via a refractive index change) as a simple linear function. We model the response cutoff as a hyperbolic tangent function to achieve a smooth transition from high response to low response. σ_c is the lower-wave number cutoff of the infrared detector, and BW (50) accounts for the width of the detector response transition. C1 is an arbitrary constant chosen to fit the data (3.25 for detector 25). The cutoff follows a linear relation with temperature:

$$\sigma_c = 1050 + 12(T - 76.324). \quad (5)$$

The analytic fit shown in Fig. 10 then has the form

$$\det 25(\sigma, T_{\mathrm{FP-hot}})/\det 25(\sigma, T_{\mathrm{FP-nom}}). \quad (6)$$

There is also a phase difference between the hot- and nominal-temperature raw spectra but the phase difference is well fit by a linear term so we may account for it in the final shift correction in Eqs. (1)–(3) when we minimize the imaginary part of the calibrated spectrum at low resolution. This temperature-driven shift is analogous to previous results from other groups [7,8].

We also examined the ratio of raw spectral amplitudes of shutter-closed (and deep-space) calibration scans at nominal optics temperature (169.79 K) and elevated temperature (169.91 K). This ratio is well fit by the ratio of Planck spectra (a self-emission effect) and there does not appear to be

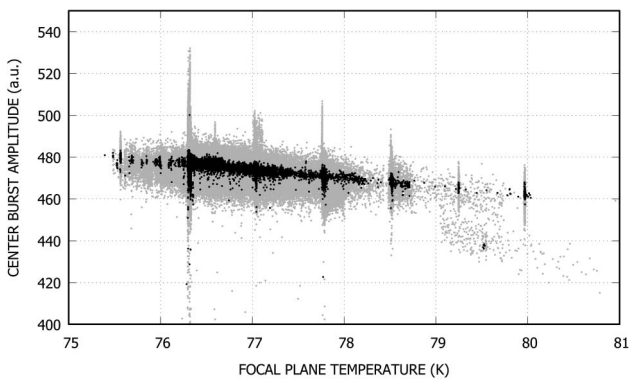

Fig. 8. 2011 shutter-closed data (black) and deep-space data (gray). The shutter-closed data have been re-scaled by a constant factor (4.74) to overlap the deep-space data.

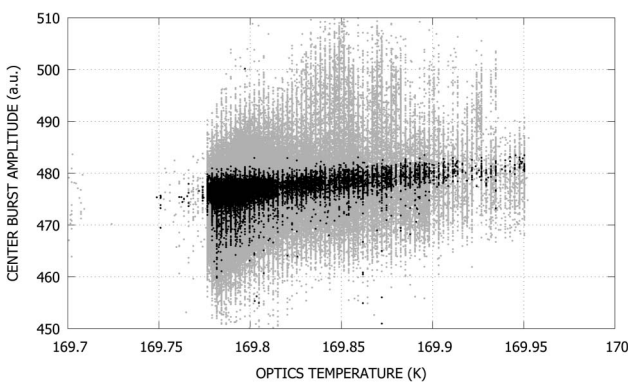

Fig. 9. 2011 shutter-closed data (black) and deep-space data (gray). The shutter-closed data have been re-scaled by a constant factor (4.74) to overlap the deep-space data.

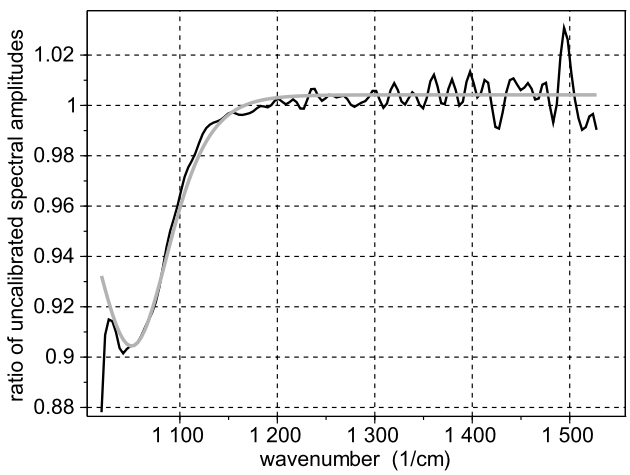

Fig. 10. Ratio of hot focal-plane temperature data to nominal temperature data (black curve) compared with an analytic fit (gray) as given by Eq. (6).

additional change due to a response change. The phase difference between hot and nominal 170 K temperature scans is negligible. Thus unlike the focal-plane temperature effect, which is a multiplicative (response) correction (applied equally to external and internal emission), the optics temperature effect is an additive effect (applied only to internal emission and not to emission from external targets). Since deep-space and shutter-closed scans include internal emission only, these scans may be corrected via multiplicative adjustments both for elevated optics temperature and for elevated focal-plane temperature.

5. INTENSITY CALIBRATION OF S3 TARGET OBSERVED WHEN CIRS NOT AT STANDARD TEMPERATURES

To incorporate the observed dependence of uncalibrated spectra on focal-plane temperature we modify Eq. (3) as follows:

$$\mathrm{calspec}_{\mathrm{FP-hot}}(\sigma) = \frac{S3\,\frac{\det 25(\sigma, T_{\mathrm{FP-nom}})}{\det 25(\sigma, T_{\mathrm{FP-hot}})} - S1}{S2 - S1} B(\sigma, T_{\mathrm{OPT-nom}}). \tag{7}$$

To incorporate the observed dependence of uncalibrated spectra on optics temperature we modify Eq. (3) in a different way:

$$\mathrm{calspec}_{\mathrm{OPT-hot}}(\sigma) = \frac{S3 - S1\,\frac{B(\sigma, T_{\mathrm{OPT-hot}})}{B(\sigma, T_{\mathrm{OPT-nom}})}}{S2 - S1} B(\sigma, T_{\mathrm{OPT-nom}}). \tag{8}$$

The normalized calibration equations (no units) are the same except for the lack of the final Planck term. For both Eqs. (7) and (8), S1 and S2 are 2011 calibration scans taken at nominal temperatures. The correction term in Eq. (8) has been applied to S1 where it can be done multiplicatively. An additive correction would have been necessary if applied to S3. In either case the goal is to cancel out self-emission in the numerator.

We use the normalized version of Eq. (7) to calibrate shutter-closed scans taken at elevated T_{FP} (Fig. 11). The temperature correction brings the calibration to better than 1% accuracy.

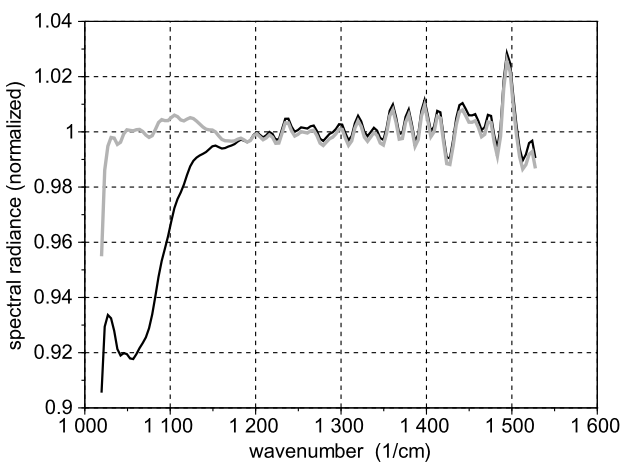

Fig. 11. Normalized spectral radiance (real part) for shutter-closed scans with elevated T_{FP}: without temperature correction (black) and with temperature correction (gray).

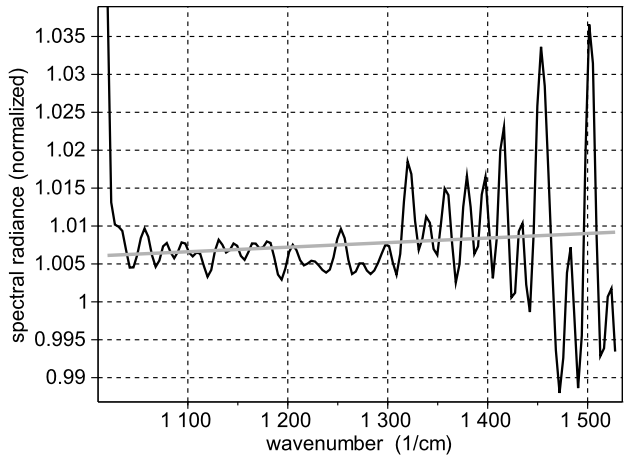

Fig. 12. Normalized spectral radiance (real part) for shutter-closed scans (black) with elevated T_{OPT}. Analytic fit (gray) based on ratio of Planck functions.

We use the normalized version of Eq. (8) to calibrate shutter-closed scans at elevated T_{OPT} (Fig. 12). The measured result (shown in black) agrees well with the expected result (gray). The expected result is the ratio of Planck functions at elevated T_{OPT} and nominal T_{OPT} (the condition for the calibration scans, S1 and S2).

Turbide and Smithson [7] adjust complex calibration for changing temperature conditions by accounting for ZPD shifts and changes in thermal self-emission. This paper extends that approach by applying an adjustment to the calibration response term via modeling the change in the detector response. Saggin *et al.* [8] also address phase issues rather than amplitude or response, furthermore needing a spectral area with either negligible or known B/S emission. Such an area is not needed for this work. We thus incorporate the approach of these previous works to adjust the sampling comb and the self-emission for temperature changes within a complex calibration scheme while adding an adjustment for the response term and expressing the equations in a particularly simple form.

6. SUMMARY

With appropriate pre-screening of scans (for bad reaction-wheel rates, for elevated telescope temperatures, for isolated scans with ZPD offsets), it is possible to implement a simple global-calibration scheme. The scheme uses large averages of the two-sided parts of calibration scans taken at nominal temperatures, which account for the majority of calibration scans. We then calibrate science-target scans at elevated (or nominal) temperatures using simple adjustments that depend only on the measured focal-plane temperature and the optics temperature in the MIR FTS near the 80 K stage. Adjustments are also made for sampling-comb changes in the science target scans due to long-term drift, laser-mode change, and temperature effects by nulling out the imaginary part of low-resolution, calibrated spectra. This local tuning of science target scans to grand-average conditions of the calibration scans (or vice versa) provides a reliably robust way of calibrating target scans taken at atypical instrument temperatures unlike a local calibration scheme, which

sometimes suffers from an inadequate number of nearby, matching calibration scans.

Funding. National Aeronautics and Space Administration (NASA) ; Cassini Mission; CIRS investigation.

Acknowledgment. We thank the CIRS calibration team for their consistent and longstanding support.

REFERENCES

1. V. Kunde, P. Ade, R. Barney, D. Bergman, J. F. Bonnal, R. Borelli, D. Boyd, J. Brasunas, G. Brown, S. Calcutt, R. Courtin, J. Cretolle, J. Crooke, M. Davis, S. Edberg, R. Fettig, M. Flasar, D. Glenar, S. Graham, J. Hagopian, C. Hakun, P. Hayes, L. Herath, L. Horn, D. Jennings, G. Karpati, C. Kellebenz, B. Lakew, J. Lindsey, J. Lohr, J. Lyons, R. Martineau, A. Martino, M. Matsumura, J. McCloskey, T. Melak, G. Michel, A. Morell, C. Mosier, L. Pack, M. Plants, D. Robinson, L. Rodriguez, P. Romani, W. Schaefer, S. Schmidt, C. Trujillo, T. Vellacott, K. Wagner, and D. Yun, "Cassini infrared Fourier spectroscopic investigation," Proc. SPIE **2803**, 162–177 (1996).
2. F. M. Flasar, V. G. Kunde, M. M. Abbas, R. K. Achterberg, P. Ade, A. Barucci, B. Bezard, G. L. Bjoraker, J. C. Brasunas, S. Calcutt, R. Carlson, C. J. Cesarsky, B. J. Conrath, A. Coradini, R. Courtin, A. Coustenis, S. Edberg, S. Edgington, C. Ferrari, T. Fouchet, D. Gautier, P. J. Gierasch, K. Grossman, P. Irwin, D. E. Jennings, E. Lellouch, A. A. Mamoutkine, A. Marten, J. P. Meyer, C. A. Nixon, G. S. Orton, T. C. Owen, J. C. Pearl, R. Prange, F. Raulin, P. L. Read, P. N. Romani, R. E. Samuelson, M. E. Segura, M. R. Showalter, A. A. Simon-Miller, M. D. Smith, J. R. Spencer, L. J. Spilker, and F. W. Taylor, "Exploring the Saturn system in the thermal infrared: the composite infrared spectrometer," Space Sci. Rev. **115**, 169–297 (2004).
3. J. C. Brasunas and B. Lakew, "Long-term stability of the Cassini Fourier transform spectrometer en route to Saturn," in *Recent Research Developments in Optics*, A. Gayathri, ed. (Research Signpost, 2004), Vol. **4**, pp. 95–113.
4. H. E. Revercomb, H. Buijs, H. B. Howell, D. D. Laporte, W. L. Smith, and L. A. Sromovsky, "Radiometric calibration of IR Fourier transform spectrometers: solution to a problem with the high-resolution interferometer sounder," Appl. Opt. **27**, 3210–3218 (1988).
5. G. Bianchini, L. Palchetti, and B. Carli, "Vectorial combination of signals in Fourier transform spectroscopy," Infrared Phys. Technol. **52**, 19–21 (2009).
6. J. Brasunas, A. Mamoutkine, and N. Gorius, "Identifying sampling comb changes in Fourier transform spectrometers with significant self-emission and beam splitter absorption," Appl. Opt. **54**, 5461–5468 (2015).
7. S. Turbide and T. Smithson, "Calibration algorithm for Fourier transform spectrometer with thermal instabilities," Appl. Opt. **49**, 3411–3417 (2010).
8. B. Saggin, D. Scaccabarozzi, and M. Tarabini, "Instrumental phase-based method for Fourier transform spectrometer measurements processing," Appl. Opt. **50**, 1717–1725 (2011).